Granulation in an atomic Bose-Einstein condensate

M. C. Tsatsos[1], J. H. V. Nguyen[2], A. U. J. Lode[3 4 5], G. D. Telles[1], D. Luo[2], V. S. Bagnato[1], & R. G. Hulet[2]

[1]*Institute of Physics of São Carlos, University of São Paulo, PO Box 369, 13560-970, São Carlos, SP, Brazil*

[2]*Department of Physics and Astronomy and Rice Quantum Institute, Rice University, Houston, Texas 77005, USA*

[3]*Department of Physics, University of Basel, Klingelbergstrasse 82, CH-4056 Basel, Switzerland*

[4]*Wolfgang Pauli Institute c/o Faculty of Mathematics, University of Vienna, Oskar-Morgenstern Platz 1, 1090 Vienna, Austria*

[5]*Vienna Center for Quantum Science and Technology, Atominstitut, TU Wien, Stadionallee 2, 1020 Vienna, Austria*

Granular matter is a multifaceted state that combines properties and aspects of all phases of matter[1]. Granulation, the process through which grains are formed in initially ordered systems, is encountered in diverse systems extending over many length and energy scales[2–4]. Granular states have been hypothesized to emerge in strongly perturbed atomic Bose-Einstein condensates[5] (BECs) as particle conglomerations but no further theoretical investigation or experimental verification exists. Here, we establish and characterize this new state of granular quantum matter in a strongly perturbed gas of bosons that – in analogy to conventional granulated matter – exhibits signatures of different quantum phases. We reach the granular

state by periodically driving the gas via a modulated scattering length[6] and study, experimentally and theoretically, the principal characteristics of unidimensional granulation in three-dimensional BECs. Grains are long-lived quantum objects whose spatial coherence is partially lost. We demonstrate that granulation is a manifestation of fluctuations in a quantum system out of equilibrium, whose description goes beyond conventional mean-field (MF) approaches. Our work thus exemplifies the hybrid nature of a BEC: emergent nonlinearities[7] coexist with probabilistic quantum mechanical behaviour[8]. We anticipate that our results will provide a more thorough understanding of the fundamental physics of phases of perturbed quantum matter and the transitions between them.

Pattern formation is a process in which an instability drives a system away from an equilibrium homogeneous state to a modulated one[9]. For instance, propagating nonlinear waves, triggered by temporal modulations of the strength of particle-particle interactions, can form in gaseous BECs as analogues to Faraday waves[9,10]. Experimental[11] and theoretical investigations, using the Gross-Pitaevskii (GP) equation[12], have described their emergence as a parametric resonance and identified the dominant modes of the instability. Certain amplitudes and frequencies of the periodic driving[13] may efficiently transfer atoms from the single-particle ground state to a variety of single-particle excited states[14,15]. Such a perturbation provides a spatially stratified structure, that is attributed to the fact that time-periodic perturbations can mimic spatially disordered potentials and yield qualitatively similar distributions of the gas[16]. In an earlier experiment, an oscillating external magnetic field was used to modulate the scattering length by exploiting a Feshbach resonance, thereby probing the lowest-lying quadrupolar mode of a BEC[6]. It was found that a

large-amplitude modulation of the interparticle interaction can provide, besides excitation of collective modes, a concentration of the particles into separated regions; a phenomenon that was, however, not further scrutinized. More recently, granulation was studied within the wider context of quantum turbulence[5,17,18] in two and three spatial dimensions, and is understood as a violent process that goes beyond collective or coherent excitations. Interestingly, the one-dimensional limit discussed here, has not been hitherto examined.

Our observations (see also Ref.[5]) show that granular BECs have the following defining properties: $i)$ they are out of equilibrium incoherent states where particles conglomerate in higher-density grains interleaved by regions of very low density, $ii)$ the spatial distribution of grains is random and fluctuating (from shot to shot), $iii)$ the typical grain size is mesoscopic, i.e. comparable to the size of the system and $iv)$ the grain size is variable and of a multiscale nature.

In our setup, an elongated gas of ^{7}Li atoms is harmonically confined in a single-beam optical-dipole trap at almost zero temperature; see Methods and ref.[6] for details. The healing length ξ is $\approx 2\mu$m, which is of the same order as the oscillator length ($l_r \approx 2.4\mu$m) and the Thomas-Fermi radius ($\approx 4\mu$m) in the transverse directions and hence, radial excitations are suppressed bringing the system close to the 1D limit. To excite the BEC we apply a time-dependent magnetic field $B = B(t)$ and obtain *in-situ* images (single shots) via polarization-phase contrast imaging (PPCI)[19] after variable modulation times $t_{\rm mod}$ followed by different hold times $t_{\rm hold}$. The field $B(t) = B_{\rm av} + \delta B sin(\Omega t)$ oscillates at frequency Ω with amplitude δB around the average value $B_{\rm av}$. The resulting modulation of the scattering length $a(t)$ follows the relation[20]

$a(t) = a(B(t)) = a_{\rm bg}\left[1 + \frac{\Delta}{B(t)-B_\infty}\right]$, i.e. it periodically oscillates between the extrema a_+ and a_- around the background value $a_{\rm bg}$. B_∞ is the position of the Feshbach resonance and Δ the width of the resonance (see Methods).

Our numerical many-body (MB) calculations and simulations of the single shots[8,21] are obtained by solving the multi-configurational time-dependent Hartree for bosons equations[22,23] for the various parameter sets of the experiment (see Methods).

In Fig. 1(a) we plot the column densities of the observed granulated states. They are remarkably stable, as they persist out to 4s after switching off the modulation. A full 3D GP simulation features excitations that appear as propagating rings in the 3D plots of the density isosurfaces and as Faraday waves[10,11] in the column densities [Fig. 1(b)]. The nature, however, of the experimentally observed grains differs from the GP simulations, principally, in their random spatial distribution, their high contrast, the inter-grain spacing and the absence of any spatial periodicity (see also Fig. 3); features that do not indicate any Faraday pattern.

To shed light on the discrepancies between the experiment and the 3D GP modeling we turn to a comparison of a 1D MF (GP) model with a 1D MB theory for M=2 modes (see Methods for details). 1D densities and simulations of single shots are shown in Fig. 2(a). For the same modulating frequencies ($\Omega/2\pi = 0, 20, 60$ and 80Hz) and amplitude we plot the integrated column densities obtained from the experiment where it is seen that shot-to-shot fluctuations are considerable for larger frequencies. As a measure of the departure of our MB model from MF states we use the 2^{nd} largest eigenvalues (or occupations) $n_2^{(1)}$ and $n_2^{(2)}$ of the 1^{st} and 2^{nd} order reduced density

matrices (RDMs), respectively (see Methods), plotted in Fig. 2(c). At zero excitation only $n_1^{(1),(2)}$ are macroscopic while $n_2^{(1),(2)}$ increase substantially with Ω, heralding the loss of 1^{st} and 2^{nd} order coherence. In other words, the system cannot be considered a MF product state any longer, it is *fragmented* and cannot, by definition, be described by the GP theory. Although the transition to fragmentation is not sharp (as the natural occupations take on continuous values) in our case it is present and persistent. Generally, fragmented condensates[24] should be distinguished from granulated ones. However, we shall show that in our setup the two phenomena appear together and persist. The density-density correlation function $C^{(2)}$ (averaged over 4-5 different runs) of the experimental data offers additional insight: large Ω results in the drop – by half – of the average distance Δz over which coherence is maintained. In Ext. Data Figs. 5 the full correlation functions are plotted as functions of pairs of points (z, z') and regions of correlations and anticorrelations can be traced.

To characterize the granulated states, we count the number of peaks (after eliminating the minor ones) and their spacing and plot them in Fig. 3(a) as a function of the frequency Ω for both experiment and simulation (see Methods). We also plot the contrast $\mathcal{D}$ (deviation of a given shot from a parabolic fit – see Methods and Ext. Data Fig. 3) of each distribution in Fig 3(b). We identify a threshold value for the frequency $\Omega_{th}/2\pi \approx 40$Hz beyond which grains start to form. For $\Omega < \Omega_{th}$ the gas oscillates coherently without significant deviation from a Thomas-Fermi-like envelope. The state is well described by the GP theory, as granulation and fragmentation are absent. For $\Omega > \Omega_{th}$ fragmentation becomes important when the system transitions to granulation. It is this region where the GP prediction for peak number, grain separation and constrast deviates

most, both from the experimental and MB results. A saturation in the granular profile appears in the experimental data for $\Omega/2\pi > 80$Hz, while the numerical codes become unstable for times before $t = 500ms$.

The dynamical evolution, as calculated from the MB theory, of the density and 1^{st} order spatial correlations of granulation is shown in Fig. 4. Contrary to a small-Ω modulation [Fig. 4(a)], modulating above Ω_{th} leads to fragmentation and a non-trivial correlation landscape [Fig. 4(b)]. Owing to such correlations large quantum fluctuations, elemental to the granulation of BECs, grow. The density, interpreted as the average of a large number of single shots, does not demonstrate grains; the latter emerge only in the single shots, either measured or simulated (see also Fig. 2). Hence, fragmentation and granulation appear together.

The transition to granular states, probed in frequency space, is dominated by quantum correlations and, for this reason, the GP theory fails to capture the transition at Ω_{th}. Grains that live to long times have been created for a variety of modulating frequencies (see also Ext. Data Figs. 1 and 2) and are in most cases $2-5$ healing lengths wide *in situ*. We conclude that they appear as nonlinear, many-body excitations that only exist within quantum fluctuations, similar in spirit to the quantum droplets recently found in dipolar BECs[25]. The fluctuating nature of granular states features random patterns, lacking periodicity in their distributions; granular states in temporally modulated BECs are thus distinct from both Faraday[11] and shock waves[26]. The multi-characteristic nature of quantum grains is supported by the observation of additional anomalous distributions in real and momentum spaces. Indeed, we are able to trace signatures of different co-

existing phases of perturbed quantum systems such as quantum turbulence and localization. We verified that the density in momentum space (as calculated from the MB theory) of the granulated state shows clear signs of a k^{-2} power-law scaling (see Ext. Data Fig. 5) which might indicate connections to turbulent BECs[27,28]. Additionally, the $\Omega/2\pi = 40$Hz experimental *in-situ* images fitted to the exponential curve $\sim \exp(-|x|^{\alpha})$ yield values for α as small as 1.25, for particular shots (see Ext. Data Fig. 7). Such a profile is reminiscent of Anderson localization found in non-interacting BECs[29].

Future studies on the statistics of the interference of the grains (via time-of-flight expansion) might cast light on the coherence properties of the system. Granulation fits well within the non-equilibrium critical phenomena[30] going beyond the hydrodynamic description and the presented quantum scenario can serve as a case-study to understand responses of many-body systems under strong forcing.

Methods

Experimental setup. Following our method presented in Ref.[6], ^{7}Li atoms in the $|1,1\rangle$ hyperfine state are harmonically confined in a cylindrically symmetric optical dipole trap with trap frequencies $\omega_x/2\pi = \omega_y/2\pi = 254$ Hz and $\omega_z/2\pi = 8$ Hz. A pair of coils in Helmholtz configuration is used to produce a homogenous magnetic field, B, which allows us to vary the interatomic interactions. For a given value of B the corresponding scattering length is determined from $a(t) = a_{\rm bg}\left(1 + \frac{\Delta}{B-B_\infty}\right)$, where $a_{\rm bg} = -24.5\ a_0$, $B_\infty = 736.2$ G, $\Delta = 192.3$ G[20] and a_0 the Bohr radius.

A BEC is formed with approximately 5×10^5 atoms at a field of $B_{\rm av} = 714$ G, which corresponds to a scattering length of $a = 140\ a_0$. The field is subsequently ramped down to $B_{\rm av} = 589.7$ G, corresponding to a scattering length of $8\ a_0$. An oscillation of the bias field, $B(t) = B_{\rm av} + \delta B sin(\Omega t)$, where $\delta B = 41.3$ G is introduced, which corresponds to a variation between a maximum a_+ and a minimum value a_- of the scattering length during the modulation, shorthanded $a = 8^{a_+=\ldots}_{a_-=\ldots} a_0$. Precisely, $a_+ = 16\ a_0$, $a_- = -1.0\ a_0$ in Fig. 1(a) and $a_+ = 20\ a_0$, $a_- = 0.5\ a_0$ in all others. We apply the modulation for $t_{\rm mod}$, and hold for $t_{\rm hold}$ before taking an *in-situ* image using PPCI[19]. This minimally-destructive imaging technique allows us to take multiple images with less than 2% of atoms lost per image. The plots in Figs. 1,2 and Ext. Data Figs. 1,2 and 3 have been recentered so as to compensate for residual dipole motion induced during condensation.

Numerical method. The Hamiltonian describing the problem is:

$$\mathcal{H}(t) = \mathcal{T} + \mathcal{V} + \mathcal{W}(t), \tag{1}$$

with $\mathcal{T} = -\frac{\hbar^2}{2m}\sum_i^N \nabla^2_{\mathbf{r_i}}$, $\mathcal{V} = \sum_i^N V_{\rm trap}(\mathbf{r_i})$ and $\mathcal{W} = \sum_{i<j} W(\mathbf{r}_i - \mathbf{r}_j; t)$ being the many-body kinetic, potential and interaction energy operators, respectively. We have:

$$V_{\rm trap}(\mathbf{r}) = \frac{\omega_z^2}{2}z^2 + \frac{\omega_r^2}{2}r^2 \quad \text{and} \tag{2}$$

$$W(\mathbf{r}_i - \mathbf{r}_j; t) = g(t)\delta(|\mathbf{r}_i - \mathbf{r}_j|) = g_0\left[-\beta_1 + \frac{\beta_1}{\beta_2 - \beta_3\sin(\Omega t)}\right]\delta(|\mathbf{r}_i - \mathbf{r}_j|), \tag{3}$$

where $\beta_1 = -\beta_2/(\beta_2 - 1) = |a_{bg}/a(\Omega = 0)| = 24.5/7.9$, $\beta_2 = |(B_{av} - B_\infty)/\Delta|$ and $\beta_3 = |\delta B/\Delta|$. The time-dependent interparticle interaction models the experimental modulation of the scattering length. In the experiment $\omega_r/\omega_z \approx 32$ and so the trap has a cigar shape, practically being in the 1D limit.

To solve the time-dependent Schrödinger equation for many interacting particles

$$i\hbar\frac{\partial\Psi}{\partial t} = \mathcal{H}(t)\Psi \tag{4}$$

we apply the MultiConfigurational Time-Dependent Hartree theory for Bosons (MCTDHB)[22,23] and use the MCTDH-X numerical solver[31–33] for 1D and 3D simulations. The MCTDHB theory assumes a general ansatz $\Psi = \Psi(\mathbf{R}, t)$ for the $N-$particle problem and expands it on a many-body basis $\Psi(\mathbf{R}, t) = \sum_k C_k(t)\Phi_k(\mathbf{R}, t)$, where Φ_k are all possible permanents (i.e., boson-symmetrized many-particle wavefunctions) built over a finite set of M orbitals (i.e. single-particle orthonormal states) ϕ_j and $\mathbf{R} = \{r_1, r_2, \ldots, r_N\}$. The theory goes beyond the standard mean-field approximation and incorporates fragmentation and correlation functions of any order n, $1 \leq n \leq$

N^8. Note that the M orbitals are found self-consistently and are *not a priori* chosen. Thereby, MCTDHB chooses the best set of orbitals at each time. We performed three sets of simulations with the following parameters:

1. One-dimensional system, with (dimensionless) trap frequency $\omega_{\rm com} = 0.1$, $N = 10,000$, $M = 1$ and $M = 2$ and $g^{(1D)} = g_0(N-1) = 357$. The interaction parameter is found from $g^{(1D)} = 2aN_{\rm exp}l_z/l_r^2$, where a is the experimental background value of the scattering length and $l_r = \sqrt{\hbar/(m\omega_r)}$, $l_z = \sqrt{\hbar\omega_{\rm com}/(m\omega_z)}$. The experimental trap frequencies $\omega_r = (2\pi)254$Hz, $\omega_z = (2\pi)8$Hz have been used, and $a = 7.9a_0$, $N_{\rm exp} = 5.7 \cdot 10^5$ particles and a periodic modulation of amplitude $\delta A = \beta_1\beta_3/\beta_2^2 = 0.93$ (see Eq. 3). The simulations and quantities derived from this dataset are presented in Figs. 2(a), 2(c), 3, and 4. The computation was performed on a 1D spatial grid of 4096 points. The modulating frequencies take on the values $\Omega/\omega_z = 1.25, 2.50, 3.75 \ldots, 12.5$, corresponding to $(2\pi)10, 20, 30, \ldots, 100$ Hz of the experimental setup. Due to the fast temporal modulation of the atom-atom interaction operator and the resulting strong local density modulations, the computations are numerically highly demanding. Therefore, extended convergence checks are required. We have confirmed convergence with respect to both the spatial grid density and the integration time step as well as error tolerance for frequencies up to $\Omega/\omega_z = 10$. Even though the error tolerance demanded is $10^{-11} - 10^{-10}$ (extremely high accuracy) the accumulated error in the total energy at the end of the propagation remains between $3 - 8\%$ and is somewhat larger for the natural occupations. This reflects the fact that the – spanned by $M = 2$ basis functions – Fock space is far from complete. At $\Omega/2\pi = 50$ and 100Hz we have seen, both in the GP and

MB simulations, resonant behaviours: the energy increases up to 20 times after ~ 5 modulation cycles and the density is found to occupy all available space. Convergence checks are beyond the computation capacities and the points at resonance have not been shown in the plots. The above resonant frequencies are close to the breathing oscillation ≈ 48Hz (and its first harmonic) of the mode excited and seen in Fig. 4. Such resonances do not show up in the 3D calculations. For $\Omega/2\pi = 90$Hz (100Hz) the system fragments completely and occupies the whole available Fock space after ~ 8 (~ 5) modulation cycles and hence more orbitals are needed (calculations not presented). Moreover, at these frequencies, the densities look largely granulated with very large values of the contrast $\mathcal{D}$.

2. One-dimensional set of systems with $\omega_z = 0.1$, $g_0(N-1) = 357$ for $i)$ variable number of orbitals $2 \leq M \leq 4$ and $N = 100$ and $ii)$ variable number of particles $100 \leq N \leq 50,000$ and $M = 2$ (Ext. Data Fig. 4). The rest of the parameters are identical to the dataset of paragraph 1 (see above). In all cases it was found that fragmentation persists both as a function of M and N.

3. Three-dimensional system with $\omega_z = 1, \omega_y = \omega_x = 32$, $N = 1000$, $M = 2$ and $g^{(3D)} = 4\pi N_{\rm exp} a/l_z = 222$. The computational grid was $512 \times 64 \times 64$ wide. All other parameters are set as in paragraph 1. The modulation frequency was set to $\Omega = 8.75\omega_z$, that corresponds to the experimental value $\Omega/2\pi = 70$Hz. The amplitude of modulation of the interaction is as in 1, i.e. remaining always positive (results plotted in Figs. 1).

All our simulations use a discrete variable representation. The orbital part of the MCTDHB equa-

tions of motion are solved using Runge-Kutta or Adams-Bashforth-Moulton of fixed order (between 5 and 8) and variable stepsize as well as the Bulirsch-Stoer scheme of variable order and stepsize. Davidson diagonalization and short iterative Lanczos schemes were used to evaluate the coefficient part of the MCTDHB equations. The stationary initial state Ψ_0 is found by imaginary time propagation. Subsequently, Ψ_0 is propagated in real time for the above time-dependent Hamiltonian and sets of parameter values. For the parameters chosen in the 3D simulation the time unit is $\tau = 19.9$ms and the length unit is $L = 13.5\mu$m. For the 1D simulations we have $\tau = 2$ms and $L = 4.3\mu$m. Energy is measured in units of $\hbar^2/(mL^2)$.

Quantities of interest The density matrix $\rho^{(N)} = |\Psi\rangle\langle\Psi|$ describes the N-body quantum system in state Ψ and the reduced density matrix (RDM) of order $p = 1, 2\ldots$ (partial trace of $\rho^{(N)}$) is most commonly employed and gives the p-particle probability densities. The eigenbasis of the RDMs gives information on the p^{th} order coherence of the system. In particular, if there is more than one macroscopic eigenvalues of the first (second) order RDM then the system is fragmented and first (second) order coherence is lost.

Specifically, the pth order reduced density matrix (RDM) is defined as[34]:

$$\rho^{(p)}(z_1,\ldots,z_p|z'_1,\ldots,z'_p;t) = \frac{N!}{(N-p)!}\int \Psi(z_1,\ldots,z_p,z_{p+1},\ldots,z_N;t)\times\Psi^*(z'_1,\ldots,z'_p,z_{p+1},\ldots,z_N;t)dz_{p+1}\ldots dz_N \quad (5)$$

$$= \sum_k n_k^{(p)}(t)\phi_k^{(p)}(z_1,\ldots,z_p;t)\phi_k^{(p)*}(z'_1,\ldots,z'_p;t), \quad (6)$$

where $n_k^{(p)}(t)$ are its eigenvalues and $\phi_k^{(p)}(t)$ its eigenfunctions. For $p = 1$, $n_k^{(1)}(t) \equiv n_k(t)$ are the so-called *natural occupations* of the corresponding *natural orbitals* $\phi_k^{(1)}(z;t)$. According to the

Onsager-Penrose definition[35], a system of N interacting bosons is said to be condensed if and only if one natural orbital $\phi_m^{(1)}$ is macroscopically occupied, or, $n_m/N \sim 1$ for some m, while $n_j/N \sim 0$ for $j \neq m$. If more than one natural orbital is macroscopically occupied then the system is called *fragmented*[36]. The diagonal

$$\rho(z;t) \equiv \rho^{(1)}(z|z;t) = \sum_{k=1}^{M} n_k(t)|\phi_k^{(1)}(z;t)|^2 \tag{7}$$

we simply call *density*. The eigenfunctions $\alpha_j^{NG}(z_1, z_2)$ of the 2^{nd} order RDM are known as *natural geminals* (NG). Their occupations satisfy $\sum_{j=1} n_j^{(2)} = N(N-1)$ and are plotted in Fig. 2 (normalized to 1).

The pth order correlation function is:

$$g^{(p)}(z_1, \ldots, z_p|z_1', \ldots, z_p';t) = \frac{\rho^{(p)}(z_1, \ldots, z_p|z_1', \ldots, z_p';t)}{\sqrt{\prod_{i=1}^{p} \rho^{(1)}(z_i, z_i;t)\rho^{(1)}(z_i', z_i';t)}}. \tag{8}$$

The skew diagonal (antidiagonal)

$$g_{skew}(z,t) = g^{(1)}(z, -z;t). \tag{9}$$

gives the degree of correlation of the density at a point z with its antipodal at point z'[37] (see Fig. 4). Similarly, the normalized pth order correlation function in momentum space can be defined, via the Fourier transform $\tilde{\rho}^{(p)}(k_1, \ldots, k_p|k_1', \ldots, k_p';t)$ of $\rho^{(p)}(z_1, \ldots, z_p|z_1', \ldots, z_p';t)$. Note that $|g^{(1)}|$, the spatial correlation function, is bounded like $0 \leq |g^{(1)}| \leq 1$ for any two points (z, z'). For Bose condensed and hence non-fragmented states, $|g^{(1)}|$ takes its maximal value everywhere in space and the state is first-order coherent. Moreover, if $|g^{(2)}| < 1$ we term the state *anticorrelated* while for $|g^{(2)}| > 1$ we term it *correlated*.

The *contrast parameter* $\mathcal{D}$ quantifies the deviation of some spatial distribution $n(z) = n(z;t_0)$ of a single shot at a given time t_0 from the parabolic (Thomas-Fermi-like) best fit $n_{\rm bf}(z) = n_{\rm bf}(z;t_0)$ at the same time and is defined as:

$$\mathcal{D} = \int dz \frac{|n(z) - n_{\rm bf}(z)|}{n_{\rm bf}(z)} \quad \text{or} \tag{10}$$

$$\mathcal{D} = \sum_i^{n_{\rm gp}} \frac{|n(i) - n_{\rm bf}(i)|}{n_{\rm bf}(i)}, \quad \text{iff} \quad |n(i) - n_{\rm bf}(i)| \geq C_{\rm cutoff}, \tag{11}$$

where i runs over all $n_{\rm gp}$ pixels/grid points. The cutoff requirement $C_{\rm cutoff} = 0.15\ n_{\rm bf}(0)$ is set so that small (zero-excitation) fluctuations are wiped out and only values with large deviations are considered (see Ext. Data Fig. 3). Therefore, the resulting contrast parameter reflects only the large deviations of a given density from its parabolic best fit. To determine the best fits we used the `gnuplot` software to fit the polynomial $p(z) = -a(z-b)^2 + c$, where $a, b, c \in \mathbb{R}$, to the obtained experimental or numerical distributions $n(z)$ along z. The two-dimensional experimental column densities have been integrated along y. The experimental data were also interpolated to a number of points along z so as to equal the grid used for the numerical simulations. An example of a processed image is shown in Ext. Data Fig. 3.

The *single-shot simulations* plotted in Figs. 2 and Ext. Data Fig. 3 have been obtained with the method prescribed in Refs.[8,21]. In brief, the procedure relies in sampling the many-body probability space as follows: one calculates the density $\rho_0(z)$, from the obtained solution $|\Psi^{(0)}\rangle \equiv \Psi$ of the MCTDHB equations. A random position z_1' is drawn such that $\rho_0(z_1') > p$, where p is a random number between zero and the maximum value of ρ_0. In continuation, one particle is annihilated at z_1', the reduced density ρ_1 of the reduced system $|\Psi^{(1)}\rangle$ is calculated and a new random position

z_2' is drawn. The procedure continues for $N-1$ steps and the resulting distribution of positions $(z_1', z_2', \ldots, z_N')$ simulates a single shot.

The one-dimensional density-density (auto-)*correlation function* of Fig. 2 for some observed distribution $n(z)$ is found from[38]:

$$\tilde{C}^{(2)}(\Delta z) = \left\langle \frac{\int n(z)n(z+\Delta z)dz}{\left[\int n(z)dz\right]^2} \right\rangle, \tag{12}$$

where $\langle \ldots \rangle$ indicates an average over all experimental runs for identical initial conditions and $n(z)$ the integrated 1D column densities. In Ext. Data Fig. 5 the correlation function has been calculated as

$$\tilde{C}^{(2)}_{2D}(z,z') = \frac{\langle n(z)n(z')\rangle}{\langle n(z)\rangle \langle n(z')\rangle}. \tag{13}$$

The normalized 1D (2D) $C^{(2)}$ is obtained from $C^{(2)}(z) = \tilde{C}^{(2)}(z)/\tilde{C}^{(2)}(0)$ $\left[C^{(2)}_{2D}(z,z') = \tilde{C}^{(2)}_{2D}(z,z')/\tilde{C}^{(2)}_{2D}(z=z')\right]$. An analysis of the single shot histograms shows that $C^{(2)}_{2D}(z,z')$ can be expressed as linear combination of $g^{(p)}$'s. However, the two are non-trivially connected and further investigations are necessary in this aspect.

The number of prominent peaks (that indicate the number of grains) of a given distribution (Fig. 3) has been found by counting local maxima, after the data have been normalized and smoothened out via a gaussian convolution of width $\sigma = 20(5)$ for the numerical (experimental) data. Different σ is chosen for the experiment and theory due to the different spatial resolutions and overall shapes of the available data. In that way we count only the most prominent peaks and not the small spatial fluctuations.

1. Jaeger, H. M., Nagel, S. R. & Behringer, R. P. Granular solids, liquids, and gases. *Rev. Mod. Phys.* **68**, 1259 (1996).

2. Mehta, A. (ed.) *Granular Matter: an Interdisciplinary Approach* (Springer-Verlag New York, 1994).

3. Richard, P., Nicodemi, M., Delannay, R., Ribiere, P. & Bideau, D. Slow relaxation and compaction of granular systems. *Nat. Mater.* **2**, 121 (2005).

4. Beloborodov, I., Lopatin, A. V., Vinokur, V. M. & Efetov, K. B. Granular electronic systems. *Rev. Mod. Phys.* **79**, 469 (2007).

5. Yukalov, V. I., Novikov, A. N. & Bagnato, V. S. Formation of granular structures in trapped Bose-Einstein condensates under oscillatory excitations. *Laser Phys. Lett.* **11**, 095501 (2014).

6. Pollack, S. E. *et al.* Collective excitation of a Bose-Einstein condensate by modulation of the atomic scattering length. *Phys. Rev. A* **81**, 053627 (2010).

7. Kevrekidis, P. G., Frantzeskakis, D. J. & Carretero-González, R. *Emergent nonlinear phenomena in Bose-Einstein condensates* (Springer-Verlag Berlin Heidelberg, 2008).

8. Sakmann, K. & Kasevich, M. Single-shot simulations of dynamic quantum many-body systems. *Nat. Phys.* **12**, 451 (2016).

9. Staliunas, K., Longhi, S. & de Valcárcel, G. J. Faraday patterns in Bose-Einstein condensates. *Phys. Rev. Lett.* **89**, 210406 (2002).

10. Staliunas, K., Longhi, S. & de Valcárcel, G. J. Faraday patterns in low-dimensional Bose-Einstein condensates. *Phys. Rev. A* **70**, 011601 (2004).

11. Engels, P., Atherton, C. & Hoefer, M. A. Observation of Faraday waves in a Bose-Einstein condensate. *Phys. Rev. Lett.* **98**, 095301 (2007).

12. Nicolin, A. I., Carretero-González, R. & Kevrekidis, P. G. Faraday waves in Bose-Einstein condensates. *Phys. Rev. A* **76**, 063609 (2007).

13. Vidanović, I., Balaž, A., Al-Jibbouri, H. & Pelster, A. Nonlinear Bose-Einstein condensate dynamics induced by a harmonic modulation of the s-wave scattering length. *Phys. Rev. A* **84**, 013618 (2011).

14. Yukalov, V. I., Yukalova, E. P. & Bagnato, V. S. Non-ground-state Bose-Einstein condensates of trapped atoms. *Phys. Rev. A.* **56**, 4845 (1997).

15. Clark, L. W., Gaj, A., Feng, L. & Chin, C. Collective emission of matter-wave jets from driven Bose-Einstein condensates. *arXiv* 1706.05560 (2017).

16. Yukalov, V. I., Yukalova, E. P. & Bagnato, V. S. Bose systems in spatially random or time-varying potentials. *Laser Phys.* **19**, 686 (2009).

17. Seman, J. *et al.* Route to turbulence in a trapped Bose-Einstein condensate. *Laser Phys. Lett.* **8**, 691 (2011).

18. Tsatsos, M. C. *et al.* Quantum turbulence in trapped atomic Bose-Einstein condensates. *Phys. Rep.* **622**, 1 (2016).

19. Bradley, C. C., Sackett, C. A. & Hulet, R. G. Bose-Einstein condensation of lithium: Observation of limited condensate number. *Phys. Rev. Lett.* **78**, 985 (1997).

20. Pollack, S. E. *et al.* Extreme tunability of interactions in a ^{7}Li Bose-Einstein condensate. *Phys. Rev. Lett.* **102**, 090402 (2009).

21. Lode, A. & Bruder, C. Fragmented superradiance of a Bose-Einstein condensate in an optical cavity. *Phys. Rev. Lett.* **118**, 013603 (2017).

22. Streltsov, A. I., Alon, O. E. & Cederbaum, L. S. Role of excited states in the splitting of a trapped interacting Bose-Einstein condensate by a time-dependent barrier. *Phys. Rev. Lett.* **99**, 030402 (2007).

23. Alon, O. E., Streltsov, A. I. & Cederbaum, L. S. Multiconfigurational time-dependent Hartree method for bosons: Many-body dynamics of bosonic systems. *Phys. Rev. A* **77**, 033613 (2008).

24. Mueller, E. J., Ho, T.-L., Ueda, M. & Baym, G. Fragmentation of Bose-Einstein condensates. *Phys. Rev. A* **74**, 033612 (2006).

25. Kadau, H. *et al.* Observing the Rosensweig instability of a quantum ferrofluid. *Nature* **530**, 194 (2016).

26. Pérez-García, V. M., Konotop, V. V. & Brazhnyi, V. A. Feshbach resonance induced shock waves in Bose-Einstein condensates. *Phys. Rev. Lett.* **92**, 220403 (2004).

27. Thompson, K. J. *et al.* Evidence of power law behavior in the momentum distribution of a turbulent trapped Bose-Einstein condensate. *Laser Phys. Lett.* **11**, 015501 (2014).

28. Navon, N., Gaunt, A. L., Smith, R. P. & Hadzibabic, Z. Emergence of a turbulent cascade in a quantum gas. *Nature* **539**, 72 (2016).

29. Roati, G. *et al.* Anderson localization of a non-interacting Bose–Einstein condensate. *Nature* **453**, 895 (2008).

30. Hinrichsen, H. Non-equilibrium critical phenomena and phase transitions into absorbing states. *Adv. Phys.* **49**, 815 (2000).

31. Lode, A. U. J. Multiconfigurational time-dependent hartree method for bosons with internal degrees of freedom: Theory and composite fragmentation of multicomponent Bose-Einstein condensates. *Phys. Rev. A* **93**, 063601 (2016).

32. Fasshauer, E. & Lode, A. U. J. Multiconfigurational time-dependent Hartree method for fermions: Implementation, exactness, and few-fermion tunneling to open space. *Phys. Rev. A* **93**, 033635 (2016).

33. Lode, A. U. J., Tsatsos, M. C. & Fasshauer, E. MCTDH-X: The time-dependent multiconfigurational Hartree for indistinguishable particles software (2016). http://ultracold.org.

34. Sakmann, K., Streltsov, A. I., Alon, O. E. & Cederbaum, L. S. Reduced density matrices and coherence of trapped interacting bosons. *Phys. Rev. A* **78**, 023615 (2008).

35. Penrose, O. & Onsager, L. Bose-Einstein condensation and liquid helium. *Phys. Rev.* **104**, 576 (1956).

36. Spekkens, R. W. & Sipe, J. E. Spatial fragmentation of a Bose-Einstein condensate in a double-well potential. *Phys. Rev. A* **59**, 3868 (1999).

37. Bouchoule, I., Arzamasovs, M., Kheruntsyan, K. V. & Gangardt, D. M. Two-body momentum correlations in a weakly interacting one-dimensional Bose gas. *Phys. Rev. A* **86**, 033626 (2012).

38. Tavares, P. E. S. *et al.* Chaotic nature of turbulent Bose-Einstein condensates. *arXiv:1606.01589* (2016).

Supplementary Information

Acknowledgments This work was partially supported by FAPESP through the CEPID program (Brazil), the NSF (grants PHY-1408309 and PHY-1607215), the Welch Foundation (grant C-1133), the Army Research Office Multidisciplinary University Research Initiative (grant W911NF-14-1-0003), and the Office of Naval Research (grant N000141612717). A.U.J.L. acknowledges financial support by the Swiss SNF and the NCCR Quantum Science and Technology as well as by the Austrian Science Foundation (FWF) under grant No F65 (SFB Complexity in PDEs) and the Wiener Wissenschafts- und TechnologieFonds (WWTF) project No MA16-066 (SEQUEX). We thank K. Farias for technical assistance. Special thanks to V. Yukalov for seminal ideas in the interpretation, A. Novikov and R. Kaiser for useful discussions. Computational time on the Cray XC30/XC40 Hornet/Hazel Hen supercomputer of the HLRS as well as the HPC of USP is gratefully acknowledged.

Author contributions M.C.T. and A.U.J.L. performed the theoretical modeling and provided the numerical simulations. J.H.V.N., G.D.T., V.S.B., D.L. and R.G.H. performed the experiments and collection of the data. All authors contributed to the writing of the manuscript and interpretation of the results.

Author information The authors declare no competing financial interests. Readers are welcome to comment on the online version of the paper. Correspondence and requests for materials should be addressed to R.G.H. (randy@rice.edu).

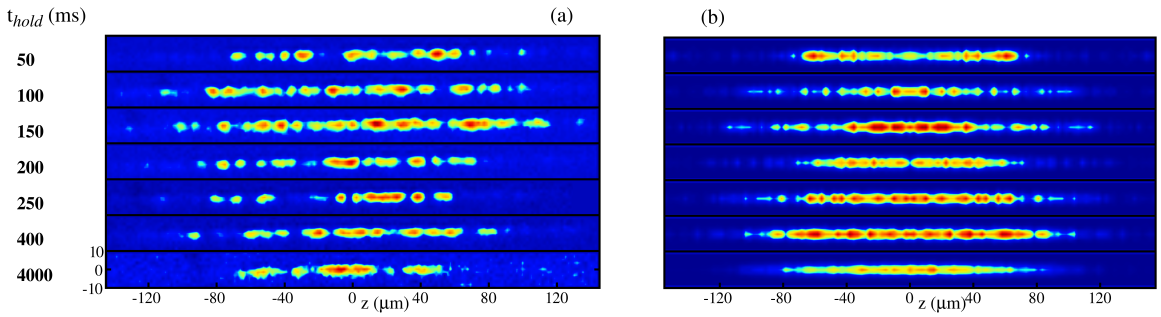

Figure 1: **Granulation of a lithium Bose-Einstein condensate in the laboratory (a) and simulation (b).** Modulating the gas for $t_{\rm mod} = 250$ms followed by relaxation for variable $t_{\rm hold}$ (as noted) leads to grain formation, that persist for times as long as $t_{\rm mod} = 4$s. The external magnetic field oscillates at $\Omega/2\pi = 70$ Hz with and amplidute of $\delta B = 41.3$G around $B_{av} = 577.4$G, inducing an oscillating scattering length of $a(t) = 8^{a_+=16}_{a_-=-1.0}\, a_0$. (a) Column densities of single *in-situ* experimental realizations (shots) are shown for various hold times. (b) GP mean-field integrated 2D column densities for the same $t_{\rm hold}$ (see text for initial conditions). The density modulations predicted by the GP mean-field theory – due to their regular distribution and low contrast – resemble Faraday waves rather than grains.

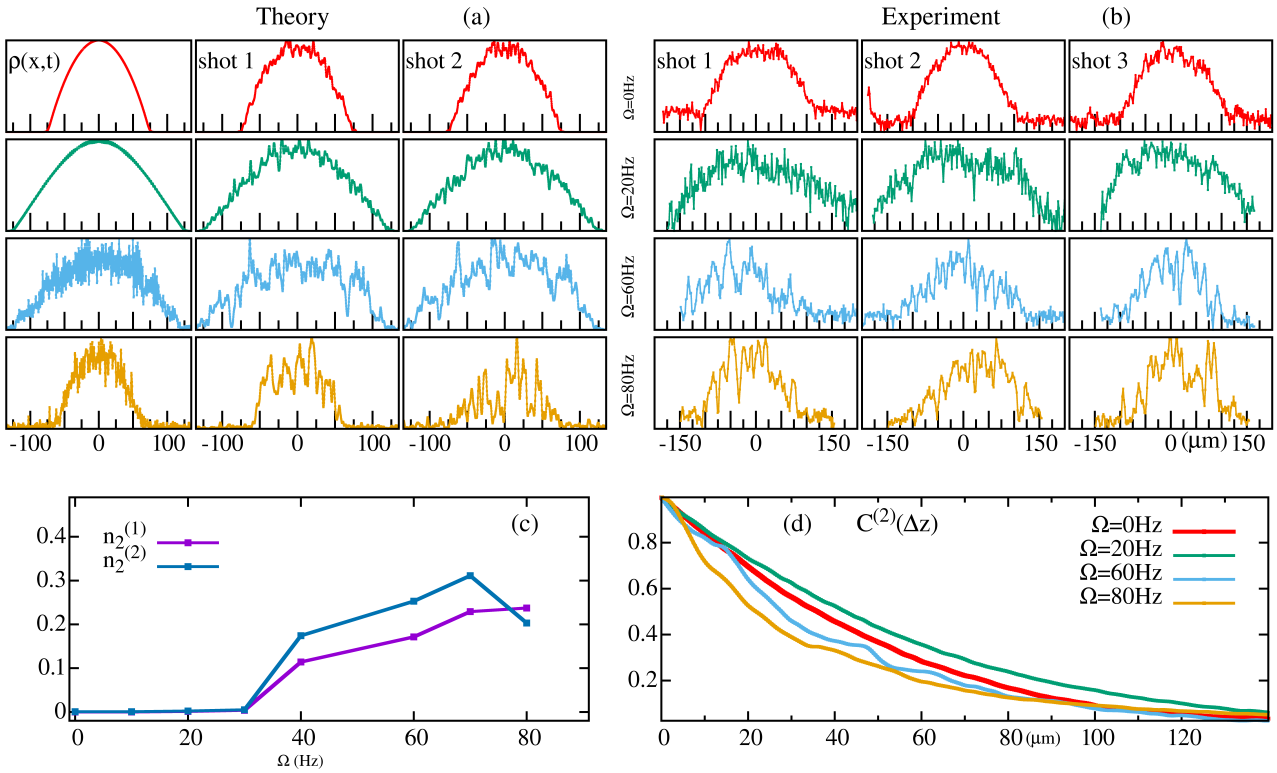

Figure 2: **Density profiles and single shots of the granulated gas.** Many-body simulations (a),(c) and experimental data (b),(d) for four different modulating frequencies Ω. (a) The first column shows the density as calculated from the 1D MB theory (see Methods) while in the second and thirds columns we plot two single shots that correspond to the experimental runs. (b) Three experimental runs for the same Ω and initial conditions as in (a) ($\delta B = 41.3$G, $B_{av} = 590.8$G, $a = 8^{a_+=20}_{a_-=0.5} a_0$ and Ω as noted). As Ω increases and grains form, shot-to-shot fluctuations become large and deviate substantially from the theoretical density. (c) Eigenvalues of the first and second order RDM (theory) and (d) density-density correlations for the experimental data (see text). The *half-length* $l_{1/2}$, at which the value of $C^{(2)}(\Delta z)$ drops to half, nearly halves as Ω goes from 0 to 80Hz. (c) and (d) underline the departure from uncorrelated mean-field states for increasing Ω. All plots are at $t = 500$ms, i.e. after 250ms of modulation and 250ms of hold time.

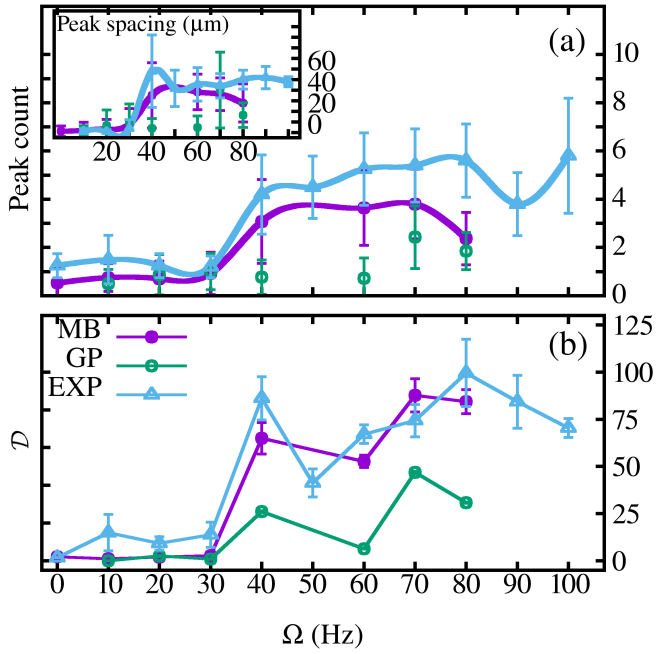

Figure 3: **Granulation vs. Ω.** (a) Comparison of the average number and spacing of grains (inset) and (b) deviations from a parabolic distribution as quantified by the contrast parameter $\mathcal{D} = \mathcal{D}(\Omega)$ (see Methods) for single shots simulated with the GP theory, the MB theory, and taken in experiment (EXP). The threshold value for $\Omega_{th}/2\pi \sim 40$Hz where deviations become large and grains form is predicted by the MB theory, while the number of grains is somewhat underestimated. The GP model fails to capture the transition to granulation at $\Omega_{th}/2\pi \sim 40$Hz. The inset shows the average spacing of the grains as a function of Ω (for the same range of frequencies). Each symbol and its error bar are the mean and standard error of the mean of at least 4 experimental measurements of $\mathcal{D}$, while 100 single shots at each Ω have been used for the GP and MB simulations.

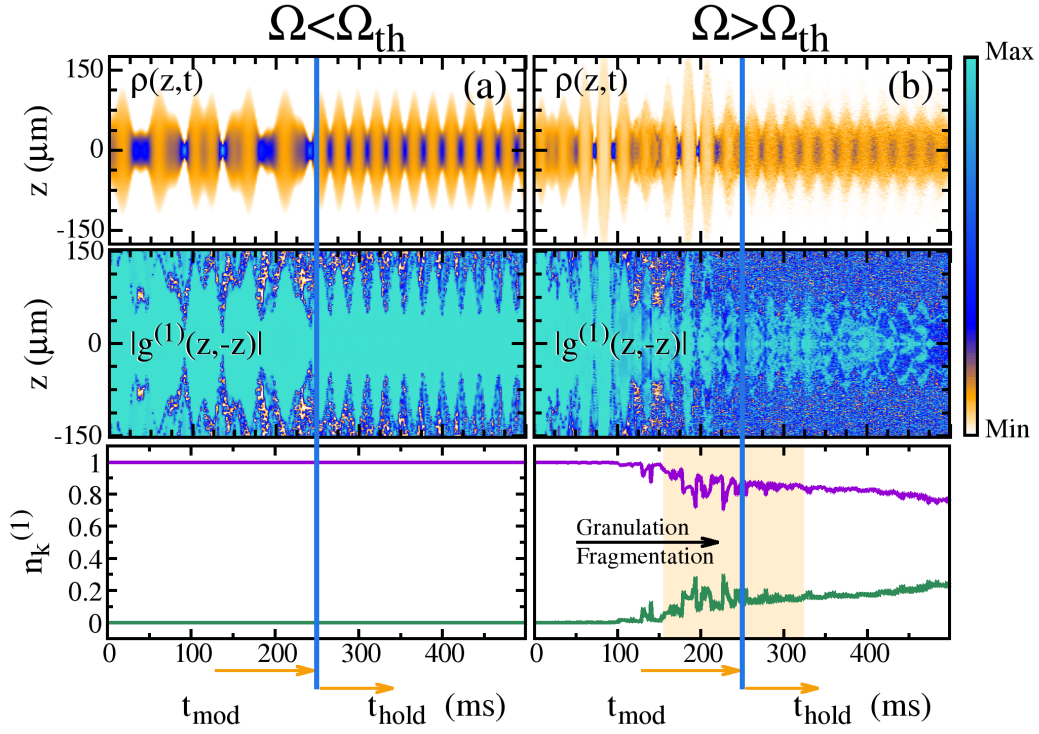

Figure 4: **Time-evolution of grains, coherence, and fragmentation.** Top downwards, we plot the density $\rho(z,t)$, first-order spatial correlation function $|g^{(1)}(z,-z)|$ and natural occupations $n_k^{(1)}(t)$ versus time t (the modulation of the interaction is switched off after $t_{\rm mod} = 250$ms). Panel (a) is calculated with $\Omega = (2\pi)20$Hz$< \Omega_{th}$ and (b) with $\Omega = (2\pi)80$Hz$> \Omega_{th}$. The shaded region marks the onset and formation of granulation and simultaneous drop in the values of $|g^{(1)}|$ and $n_1^{(1)}$. Here $\omega_z = (2\pi)8$Hz, $N = 10^4$ and $M = 2$ (see Methods). While $\Omega < \Omega_{th}$ does not affect the natural orbital occupations, $\Omega > \Omega_{th}$ results in the second natural orbital being macroscopically populated and hence in the fragmentation of the BEC.

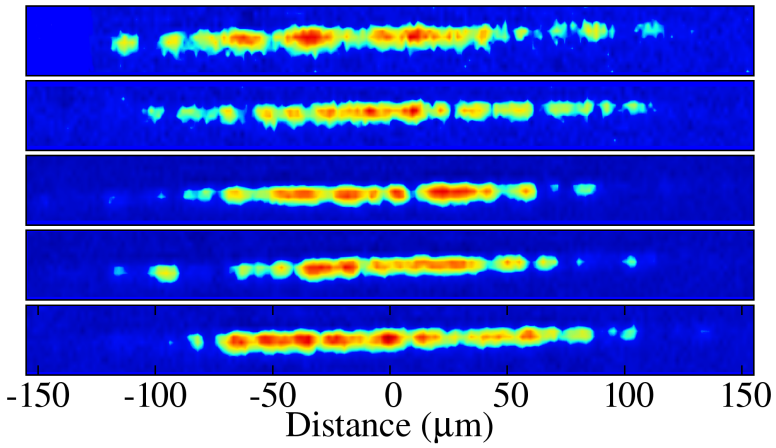

Extended Data Figure 1 | Granulation of the lithium Bose-Einstein condensate, after $\mathbf{t_{mod}} = \mathbf{250ms}$ and $\mathbf{t_{hold}} = \mathbf{250ms}$. Five different experimental realizations (shots) corresponding to identical initial conditions, namely modulating frequency $\Omega/2\pi = 60Hz$ and amplitude of the scattering length modulation $a(t) = 8^{a_+=20}_{a_-=0.5}a_0$. The fluctuations from shot to shot reveal that quantum correlations are large and underpin the emergence of granular structures.

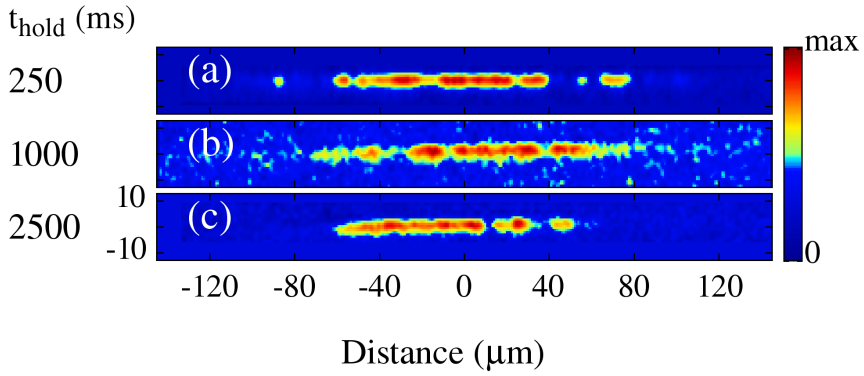

Extended Data Figure 2 | Long-time dynamics of grains. Granulation is seen in the laboratory for a variety of modulating frequencies and for long times after the excitation has been switched off (also shown in Fig. 1 and Ext. Data Fig. 1). Here $\Omega/2\pi = 70Hz$ and amplitude $a(t)$ same as in Ext. Data Fig. 1. The hold times are depicted whereas the modulation time is $t_{\rm mod} = 250$ms in (a),(c) and $t_{\rm mod} = 1000$ms in (b).

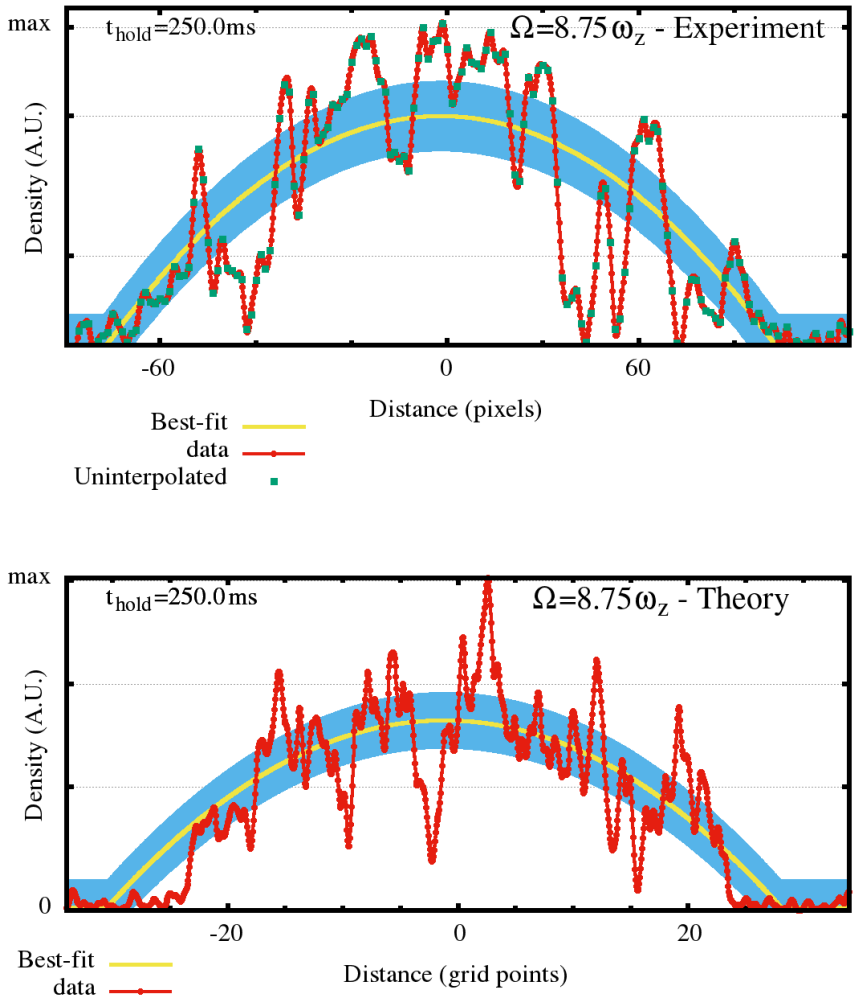

Extended Data Figure 3 | Example of data fitting. (upper) Experimental and (lower) numerical data are fitted to a parabolic curve (yellow) in order to estimate the distance (contrast $\mathcal{D}$) of the former from the latter (see Methods). Only values of $\mathcal{D}$ that deviate more than 15% from the value of the fitting function (i.e. points that lie outside the shaded area) are taken into consideration. The images are taken at $\Delta \mathrm{t} = t_{\mathrm{mod}} + t_{\mathrm{hold}} = 250 + 250$ms. The numerical simulation is a 1D model with $N = 10^4$ and $M = 2$ and the grid extension is [-128:128]. Cf. Fig 2b.

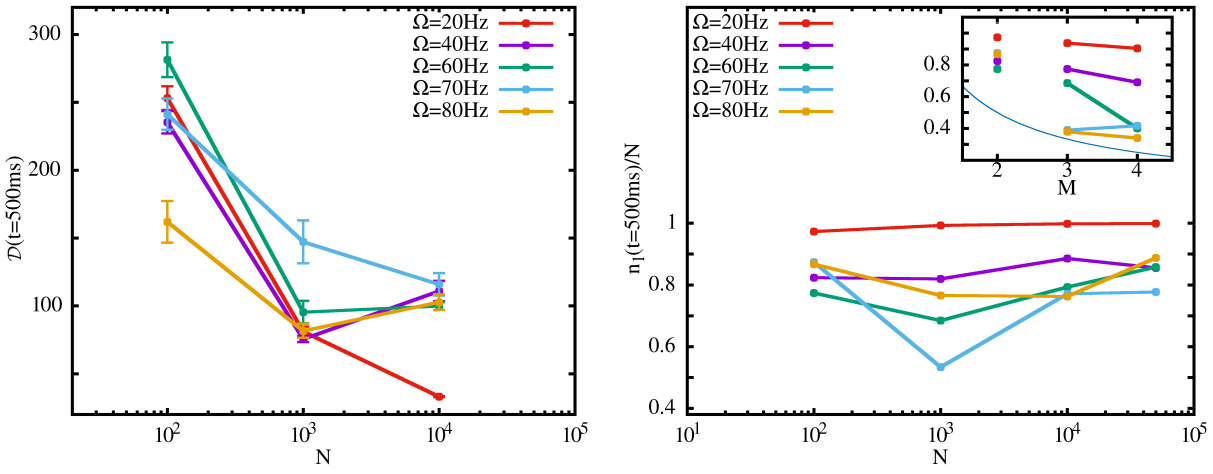

Extended Data Figure 4 | Granulation in the simulation of varying particle and orbital numbers. (left) The contrast parameter $\mathcal{D}$ (mean and error of 10 single shots) is naturally very high for low particle numbers N and drops as the latter increases. For the granulated gas ($\Omega/2\pi \geq 40$Hz) it saturates between $N = 1000$ and $N = 10000$, while it goes to almost zero for the non-granulated gas (red line – $\Omega/2\pi = 20$Hz) and large N. (right) Largest occupation number n_1 for the modulated system for different frequencies (as noted) as function of the total particle number N. For the granulated systems n_1 oscillates, in most cases, between 0.65 and 0.85 meaning that fragmentation persists to large systems. The non-granulated gas stays practically condensed ($\Omega/2\pi = 20$Hz). (inset) Occupation n_1 versus the total orbital number used M. The $y = 1/M$ blue line of the inset denotes the minimal occupation that the largest eigenvalue n_1 can have for given M. All points obtained from the 1D MB theory (see Methods) at the end of the modulation process (i.e. after $\Delta\mathrm{t} = t_{\mathrm{mod}} + t_{\mathrm{hold}} \approx 250 + 250$ms).

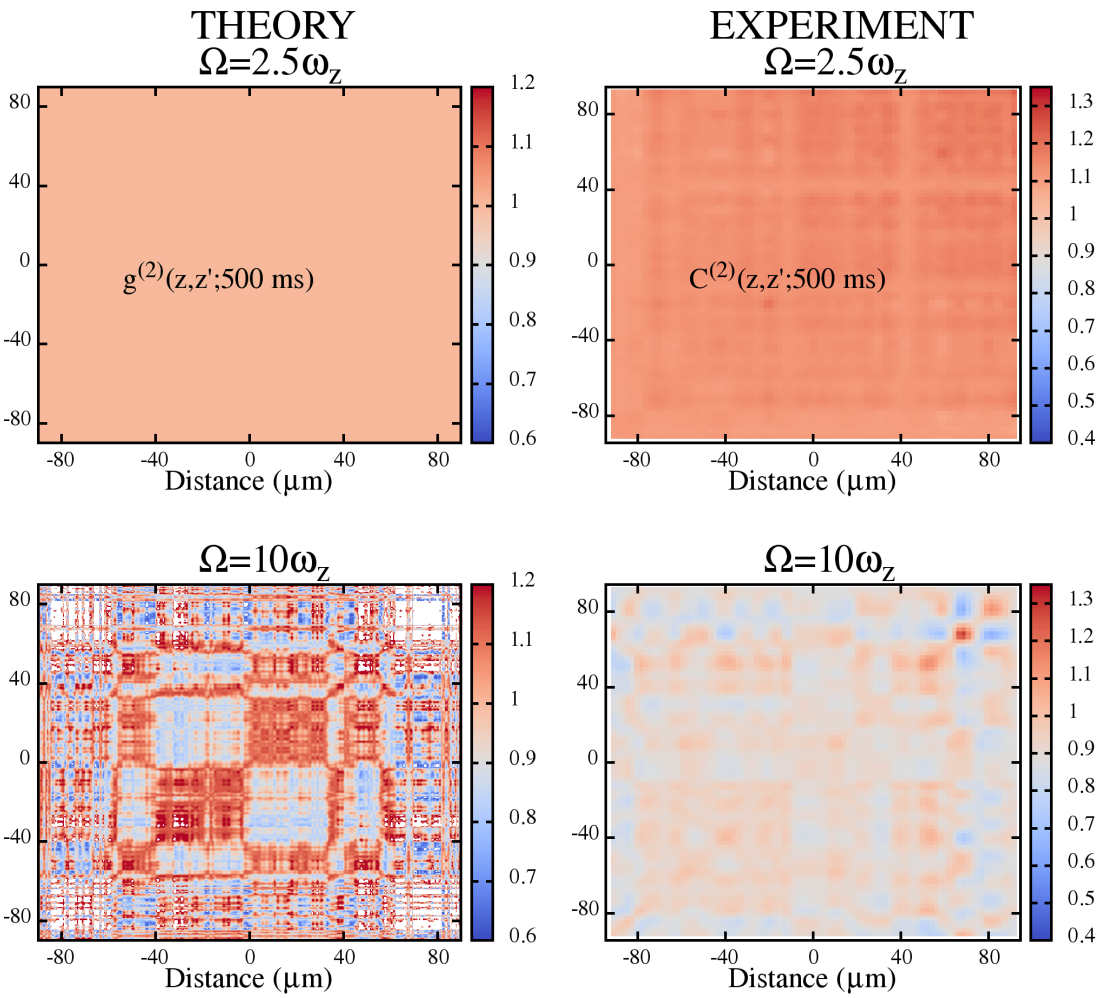

Extended Data Figure 5 | 2^{nd} order correlation functions. (left) Correlation function $g^{(2)}$ (see Methods) for the non-granulated gas modulated with frequency $\Omega = (2\pi)20Hz = 2.5\omega_z$ (upper) and the granulated gas modulated with frequency $\Omega = (2\pi)80Hz = 10\omega_z$ (lower panel), as calculated from the 1D MB theory. (right) Correlation function $C^{(2)}$ (see Methods) as calculated from the experiment for the same frequencies. The largely constant correlation plane of the non-granulated gas gives rise to regions, roughly 30μm wide, where correlations ($|g^{(2)}| > 1$, red hues) and anticorrelations ($|g^{(2)}| < 1$, blue hues) evolve, as depicted in the lower panel. All images are plotted at time $t = 500$ms, i.e. after 250ms of modulation and 250ms of hold time and modulation $a(t) = 8^{a_+=20}_{a_-=0.5} a_0$.

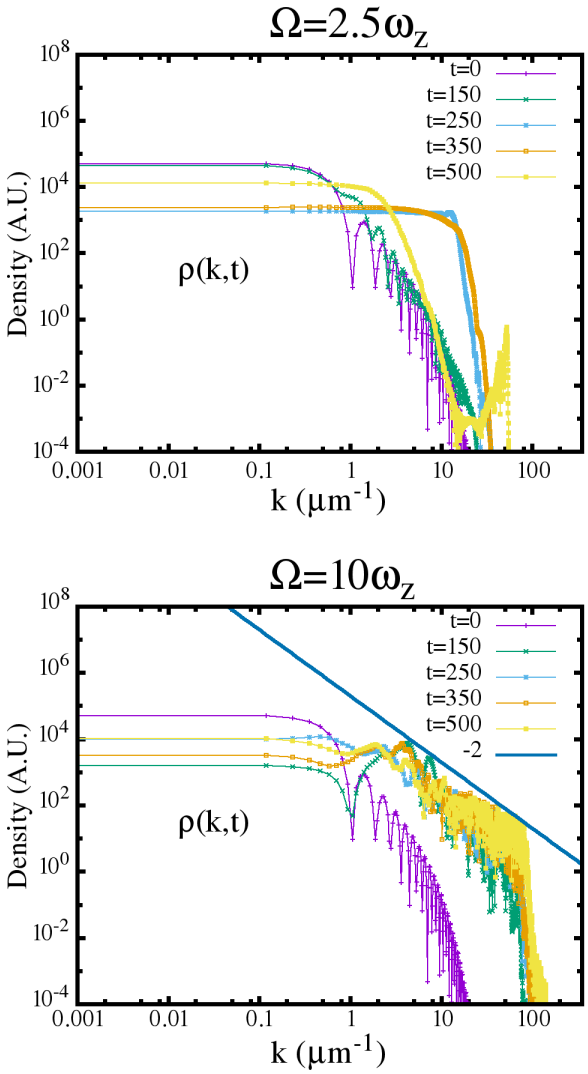

Extended Data Figure 6 | Density in momentum space. k-space densities for the regular (upper) and the granulated gas (lower panel) as calculated from the MB theory at different times (during modulation for $t \leq 250$ms and after for $t > 250$ms). In the granulated case the momentum distribution scales like k^{-2} (straight line to guide the eye) for almost two decades, behaviour that is characteristic of quantum turbulence. Contrary to the regular gas, this scaling remains even 250ms after the modulation.

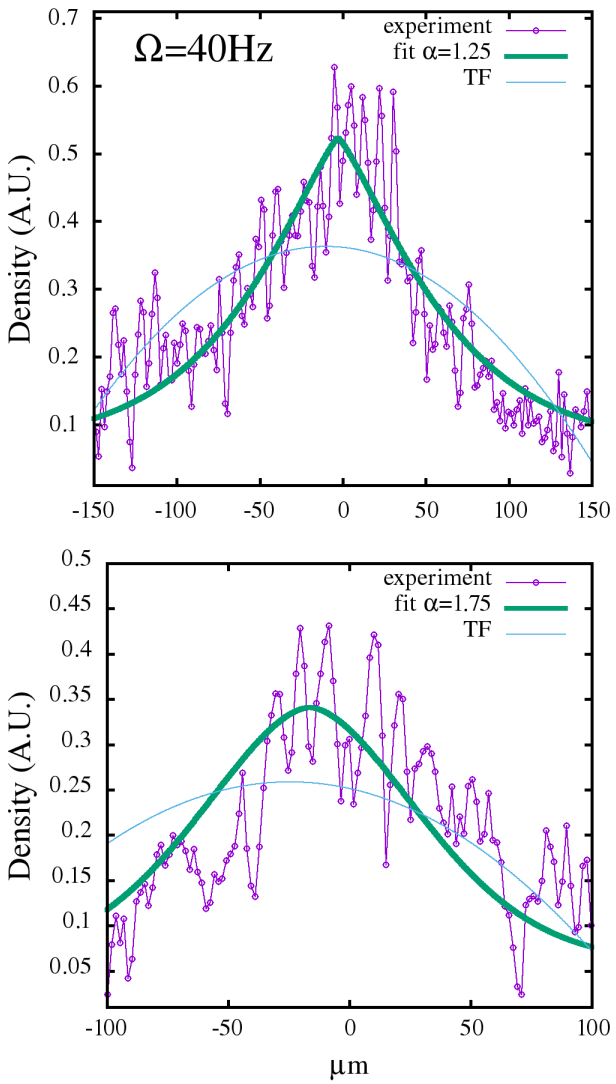

Extended Data Figure 7 | Experimental column densities exponentially fitted. Close to the threshold frequency $\Omega/2\pi = 40$Hz, where the system transits from regular to granulated states, anomalous spatial distributions are seen (here, two experimental shots for the same initial conditions). These might bear resemblance to localized states, that have been shown to exist in BECs in optical lattices[29]. We fit our observed density distributions to $C + A\exp\left(-\frac{|x-x0|^\alpha}{d}\right)$ and obtain $\alpha = 1.25$ and 1.75 for the two shots. The transition from a regular to a localized states happens as $\alpha \to 1$. For comparison, we plot the parabolic Thomas-Fermi (TF) fit (blue).